INTERNATIONAL JOURNAL FOR NUMERICAL METHODS IN FLUIDS
Int. J. Numer. Meth. Fluids 2009; **59**:1093–1110
Published online 9 July 2008 in Wiley InterScience (www.interscience.wiley.com). DOI: 10.1002/fld.1857

A semi-implicit finite volume implementation of the CSF method for treating surface tension in interfacial flows

M. Raessi, M. Bussmann*, † and J. Mostaghimi

Department of Mechanical and Industrial Engineering, University of Toronto, Toronto, Ont., Canada

SUMMARY

We present an implementation of Hysing's (*Int. J. Numer. Meth. Fluids* 2006; **51**:659–672) semi-implicit method for treating surface tension, for finite volume models of interfacial flows. Using this method, the surface tension timestep restriction, which is often very stringent, can be exceeded by at least a factor of 5 without destabilizing the solution. The surface tension force in this method consists of an explicit part, which is the regular continuum surface force, and an implicit part which represents the diffusion of velocities induced by surface tension on fluids interfaces. The surface tension force is applied to the velocity field by solving a system of equations iteratively. Since the equations are solved only near interfaces, the computational time spent on the iterative procedure is insignificant. Copyright © 2008 John Wiley & Sons, Ltd.

Received 15 August 2007; Revised 10 December 2007; Accepted 4 May 2008

KEY WORDS: surface tension; continuum surface force; interfacial flows; free-surface flows; spurious currents; volume-of-fluid; level set

1. INTRODUCTION

The continuum surface force (CSF) method [1], developed more than a decade ago, has been widely used as a model for surface tension forces in interfacial flow solvers. The CSF model is explicit, and thus for numerical stability, the timestep size Δt must satisfy the following condition:

$$\Delta t \leqslant \Delta t_{\mathrm{ST}} = \sqrt{\frac{\overline{\rho}(\Delta x)^3}{2\pi\sigma}} \tag{1}$$

where $\overline{\rho}$ is the average density of two phases, σ is the coefficient of surface tension, and Δx is the mesh size. If the viscous and convective effects are also modeled by an explicit approach, then Δt

*Correspondence to: M. Bussmann, Department of Mechanical and Industrial Engineering, University of Toronto, 5 King's College Road, Toronto, Ont., Canada M5S 3GB.
†E-mail: bussmann@mie.utoronto.ca

must also satisfy the following conditions:

$$\Delta t \leqslant \Delta t_{\text{vis.}} = \frac{\rho(\Delta x)^2}{2\mu} \tag{2}$$

where μ is fluid viscosity, and

$$\Delta t \leqslant \Delta t_{\text{CFL}} = \frac{\Delta x}{u_{\max}} \tag{3}$$

which is the Courant–Friedrichs–Lewy (CFL) condition, where $u_{\max}$ represents some maximum velocity.

Condition (1) often imposes a stringent constraint on Δt, especially if surface tension is a dominant force, e.g. when the Weber number $\text{We} = \rho L u^2/\sigma < 1$ or the capillary number $\text{Ca} = \mu u/\sigma < 1$, where L and u are the characteristic length and velocity, respectively. To compare these timestep restrictions, consider a 100 μm water droplet moving at 1 m/s, discretized by 20 cells per radius ($\Delta x = 2.5\,\mu\text{m}$, $\text{We} = 1.4$, and $\text{Ca} = 0.014$). The timestep restrictions are

$$\Delta t_{\text{ST}} = 2.5 \times 10^{-7}\,\text{s}$$

$$\Delta t_{\text{vis.}} = 8 \times 10^{-6}\,\text{s}$$

$$\Delta t_{\text{CFL}} = 2.5 \times 10^{-6}\,\text{s}$$

As we see, the timestep restriction due to surface tension is an order of magnitude smaller than the others. If this restriction could be removed, or at least mitigated, then time marching could be done at larger timesteps, and simulation runtimes would be significantly reduced. Of course, we should note that by using a large timestep, one may not be able to accurately capture and resolve all temporal attributes of a problem. For example, if the timestep were to approach the oscillation period of a drop, then obviously the solver would not capture those oscillations properly.

Hysing [2] recently reported a semi-implicit approach to the CSF model, where Δt_{ST} can be exceeded by at least a factor of 10. He presented his method in a finite element context and incorporated it into an extended version of the FEATFLOW [3] solver, where the level set (LS) method is used to represent fluid interfaces. An equally common group of flow solvers are finite volume models on Cartesian grids that employ the volume-of-fluid (VOF) method for interfacial flows (e.g. RIPPLE [4], SURFER [5], and Gerris [6]). Applying Hysing's model would be of great benefit for such solvers, as computational time could be reduced significantly; however, the extension of this method is not straightforward. In this paper, we present an implementation of Hysing's model for a VOF-based finite volume method; although, this implementation could also be applied to finite volume models that employ other interface tracking techniques, such as the LS method.

2. MATHEMATICAL FUNDAMENTALS

Consider a two-phase flow where the fluids are immiscible and incompressible. The governing equations are conservation of mass and momentum:

$$\nabla \cdot \mathbf{U} = 0 \tag{4}$$

$$\frac{\partial(\rho \mathbf{U})}{\partial t} + \nabla \cdot (\rho \mathbf{U}\mathbf{U}) = -\nabla p + \nabla \cdot (\mu(\nabla \mathbf{U} + \nabla^{\text{T}}\mathbf{U})) + \mathbf{F}_B + \mathbf{F}_{\text{ST}} \tag{5}$$

DOI: 10.1002/fld

where $\mathbf{U}$ denotes the velocity, p the pressure, $\mathbf{F}_B$ any body forces such as gravity, and $\mathbf{F}_{\mathrm{ST}}$ the surface tension force.

Using a first-order scheme to discretize the temporal derivative in Equation (5), and employing a two-step projection method, we solve Equation (5) by splitting it into predictor and corrector steps:

$$\frac{\rho^{n+1}\mathbf{U}^* - \rho^n \mathbf{U}^n}{\Delta t} = -\nabla\cdot(\rho\mathbf{U}\mathbf{U})^n + \nabla\cdot(\mu(\nabla\mathbf{U} + \nabla^{\mathrm{T}}\mathbf{U}))^n + \mathbf{F}_{\mathrm{B}}^n + \mathbf{F}_{\mathrm{ST}}^{n+1} \tag{6}$$

$$\frac{\rho^{n+1}\mathbf{U}^{n+1} - \rho^{n+1}\mathbf{U}^*}{\Delta t} = -\nabla p^{n+1} \tag{7}$$

where superscripts n and $n+1$ denote the current and next time levels, and $*$ represents an interim level.

In the CSF formulation [1],

$$\mathbf{F}_{\mathrm{ST}} = \sigma\kappa\hat{n}\delta_\Gamma \tag{8}$$

where Γ denotes an interface between two fluids, κ the interface curvature, $\hat{n}$ a unit normal vector to Γ, and δ_Γ the Dirac delta function which is used to represent Γ.

Following [2], an identity mapping, denoted as id_Γ, is defined on Γ as

$$\mathrm{id}_\Gamma = \mathbf{x}|_\Gamma = \mathbf{x}\delta_\Gamma$$

where $\mathbf{x}$ denotes the position vector. From differential geometry,

$$\underline{\Delta}\mathrm{id}_\Gamma = \kappa\hat{n} \tag{9}$$

where $\underline{\Delta}$ is the tangential (or surface) Laplacian operator, also known as the Laplace–Beltrami operator (see Appendix A). Thus, $\mathbf{F}_{\mathrm{ST}}$ becomes

$$\mathbf{F}_{\mathrm{ST}} = \sigma(\underline{\Delta}\mathrm{id}_\Gamma)\delta_\Gamma \tag{10}$$

and the surface tension term in Equation (5) can be expressed as

$$\mathbf{F}_{\mathrm{ST}}^{n+1} = \sigma(\underline{\Delta}\mathrm{id}_\Gamma^{n+1})\delta_\Gamma \tag{11}$$

where id_Γ^{n+1} denotes the interface location at time $n+1$.

Following [2, 7], a backward Euler scheme can be used to approximate id_Γ^{n+1} as

$$\mathrm{id}_\Gamma^{n+1} = \mathrm{id}_\Gamma^n + \Delta t\mathbf{U}^{n+1} \tag{12}$$

which is analogous to

$$\mathbf{x}|_\Gamma^{n+1} = \mathbf{x}|_\Gamma^n + \Delta t\mathbf{U}^{n+1} \tag{13}$$

Substituting Equation (12) into Equation (11) and rearranging, we obtain

$$\mathbf{F}_{\mathrm{ST}}^{n+1} = \sigma(\kappa\hat{n})^n\delta_\Gamma + \sigma\Delta t(\underline{\Delta}\mathbf{U}^{n+1})\delta_\Gamma \tag{14}$$

DOI: 10.1002/fld

Before proceeding, note that id_Γ^{n+1} can also be approximated via the Crank–Nicolson scheme

$$\mathrm{id}_\Gamma^{n+1} = \mathrm{id}_\Gamma^n + \frac{\Delta t}{2}(\mathbf{U}^n + \mathbf{U}^{n+1}) \tag{15}$$

which then yields an alternative to Equation (14)

$$\mathbf{F}_{\mathrm{ST}}^{n+1} = \sigma(\kappa\hat{n})^n \delta_\Gamma + \frac{\sigma\Delta t}{2}(\underline{\Delta}\mathbf{U}^n + \underline{\Delta}\mathbf{U}^{n+1})\delta_\Gamma \tag{16}$$

We will consider both Equations (14) and (16) in what follows. The term $\sigma(\kappa\hat{n})^n\delta_\Gamma$ in Equations (14) and (16) is the CSF force (see Equation (8)). Since $\sigma(\kappa\hat{n})^n\delta_\Gamma$ is evaluated at time level n, this approach is semi-implicit; therefore, there is a limit on the maximum possible Δt. It will be shown in Section 4 that the maximum Δt is at least five times Δt_{ST}. From here on, however, we will simply refer to this approach as the implicit method for ease of presentation. The additional term in Equations (14) and (16) (see Appendix A for $\underline{\Delta}\mathbf{U}$) appears as the diffusion of velocities induced by the surface tension force on an interface. Note that as Δt tends to zero, the diffusive term vanishes and the implicit method approaches the familiar explicit implementation of the CSF model.

We will substitute both forms of $\mathbf{F}_{\mathrm{ST}}^{n+1}$, Equations (14) and (16), into Equation (6), but first we rewrite Equation (6) as

$$\rho^{n+1}\mathbf{U}^* = \widetilde{\rho\mathbf{U}} + \Delta t\mathbf{F}_{\mathrm{ST}}^{n+1} \tag{17}$$

where

$$\widetilde{\rho\mathbf{U}} = \rho^n\mathbf{U}^n + \Delta t[-\nabla\cdot(\rho\mathbf{U}\mathbf{U})^n + \nabla\cdot(\mu(\nabla\mathbf{U} + \nabla^{\mathrm{T}}\mathbf{U}))^n + \mathbf{F}_{\mathrm{B}}^n] \tag{18}$$

Now substituting Equation (14) into Equation (17), we have

$$\rho^{n+1}\mathbf{U}^* = \widetilde{\rho\mathbf{U}} + \sigma\Delta t(\kappa\hat{n})^n\delta_\Gamma + \sigma(\Delta t)^2(\underline{\Delta}\mathbf{U}^*)\delta_\Gamma \tag{19}$$

In two-dimensional (2D) Cartesian coordinates, where we define $\mathbf{U} = u\hat{i} + v\hat{j}$ and the unit normal to Γ as $\hat{n} = n_1\hat{i} + n_2\hat{j}$, and using Equation (A11) for $\underline{\Delta}\mathbf{U}^*$, we obtain the following equation for applying surface tension to the u-component of velocity:

$$\begin{aligned}\rho^{n+1}u^* = \widetilde{\rho u} + \sigma\Delta t(\kappa n_1)^n\delta_\Gamma + \sigma(\Delta t)^2[n_2^2u_{xx}^* + n_1^2u_{yy}^* - 2n_1n_2u_{xy}^* \\ - (n_1u_x^* + n_2u_y^*)(n_2^2n_{1x} + n_1^2n_{2y} - n_1n_2(n_{1y} + n_{2x}))]\delta_\Gamma\end{aligned} \tag{20}$$

where $\widetilde{\rho u}$ is the x-component of Equation (18), and the subscripts x and y denote derivatives with respect to x and y, respectively. Similarly, for the v-component of $\mathbf{U}^*$, we have

$$\begin{aligned}\rho^{n+1}v^* = \widetilde{\rho v} + \sigma\Delta t(\kappa n_2)^n\delta_\Gamma + \sigma(\Delta t)^2[n_2^2v_{xx}^* + n_1^2v_{yy}^* - 2n_1n_2v_{xy}^* \\ - (n_1v_x^* + n_2v_y^*)(n_2^2n_{1x} + n_1^2n_{2y} - n_1n_2(n_{1y} + n_{2x}))]\delta_\Gamma\end{aligned} \tag{21}$$

These equations yield u^* and v^* at each timestep by solving systems of algebraic equations (presented next).

DOI: 10.1002/fld

Finally, a similar equation for $\mathbf{U}^*$ can be obtained by substituting Equation (16) (the Crank–Nicolson scheme) into Equation (17)

$$\rho^{n+1}\mathbf{U}^* = \widetilde{\rho\mathbf{U}} + \sigma\Delta t(\kappa\hat{n})^n\delta_\Gamma + \frac{\sigma(\Delta t)^2}{2}(\underline{\Delta}\mathbf{U}^n + \underline{\Delta}\mathbf{U}^*)\delta_\Gamma \tag{22}$$

which can also be expressed in terms of u^* and v^*, similar to Equations (20) and (21).

3. NUMERICAL METHODOLOGY

3.1. Solving the flow equations

Using a two-step projection method, Equations (4) and (5) are solved in 2D Cartesian coordinates. In the predictor step (Equation (6)), an interim velocity $\mathbf{U}^*$ is calculated by considering convective, viscous terms, surface tension and body forces. Then, applying Equation (4) to $\mathbf{U}^{n+1}$ in the corrector step (Equation (7)) yields an implicit equation for pressure

$$\frac{1}{\Delta t}\nabla\cdot(-\rho^{n+1}\mathbf{U}^*) = -\nabla^2 p^{n+1} \tag{23}$$

At each timestep, Equation (23) is solved iteratively for a pressure field that is then used to evaluate $\mathbf{U}^{n+1}$ via Equation (7).

A co-located arrangement of variables was used with pressure and velocities defined at cell centers. By incorporating a consistent mass and momentum advection scheme [8], the flow model can simulate high-density ratio flows. In addition to the implicit implementation of surface tension presented in Section 2, we also implemented the original [1] and consistent explicit CSF [9] models for comparison.

In the explicit models, surface tension forces are calculated at cell faces, and then averaged to cell centers. In the implicit model, however, the forces are calculated and applied at cell centers via Equations (20) and (21). These equations need to be solved only near fluid interfaces, where $\delta_\Gamma \neq 0$ (see Section 3.3 for discretization of δ_Γ). Treating fluids across an interface uniformly, we discretized the derivatives in Equations (20) and (21) via a second-order central differencing scheme, without explicitly enforcing any jump condition. This resulted in an algebraic system of equations with nine diagonals for each velocity component. In this system, the coefficient matrix is diagonally dominant because fluid density appears in the main diagonal. The matrix depends only on the topology of an interface, Δt, and σ; the orientation of the flow field relative to the interface does not influence the matrix. The explicit part of the surface tension force and $\widetilde{\rho\mathbf{U}}$ (see Equations (19) and (22)) are source terms in these systems of equations. We used LASPack [10] to solve the systems iteratively at each timestep.

3.2. Calculating interface dynamics

We employed the 'coupled LS and VOF' (CLSVOF) method of Son and Hur [11] for calculating interface dynamics, because of the relative ease of implementation compared with other CLSVOF methods. In this method, the interface is represented by a smooth LS function [12] denoted by ϕ. For a domain Ω, ϕ is defined as a signed distance function to the boundary (interface) Γ

$$|\phi(\mathbf{x})| = \min(|\mathbf{x}-\mathbf{x}_\mathrm{I}|) \quad \text{for all } \mathbf{x}_\mathrm{I}\in\Gamma \tag{24}$$

DOI: 10.1002/fld

implying that $\phi(\mathbf{x})=0$ on Γ. Choosing ϕ to be positive inside Ω, we then have

$$\phi(\mathbf{x})=\begin{cases}>0, & \mathbf{x}\in\Omega\\ 0, & \mathbf{x}\in\Gamma\\ <0, & \mathbf{x}\notin\Omega\end{cases} \tag{25}$$

The motion of the interface is defined by the following advection equation:

$$\frac{\partial\phi}{\partial t}+\mathbf{U}\cdot\nabla\phi=0 \tag{26}$$

When ϕ is advected, the $\phi=0$ contour moves at the correct interface velocity; however, contours of $\phi\neq 0$ do not necessarily remain as distance functions. This can result in an irregular ϕ field that in turn leads to problems with mass conservation. To rectify this problem reinitialization methods have been developed, which restore ϕ to a signed distance function without changing the $\phi=0$ contour.

To reinitialize ϕ in the CLSVOF method, the LS function is coupled with the VOF function. The VOF function, a scalar color function denoted by f, is defined as

$$f(\mathbf{x})=\begin{cases}1, & \mathbf{x}\in\text{fluid 1}\\ 0, & \mathbf{x}\in\text{fluid 2}\end{cases} \tag{27}$$

to represent fluid 1 in a two-fluid system. The VOF function is advected by

$$\frac{\partial f}{\partial t}+\mathbf{U}\cdot\nabla f=0 \tag{28}$$

After advecting ϕ and f from time n to $n+1$, the interface, approximated as piecewise linear, is then reconstructed from f^{n+1} using the interface normal vectors calculated from ϕ^{n+1}. ϕ is then reinitialized by calculating the distance between any cell center (where ϕ is defined) and the VOF interface.

The CLSVOF method achieves exact volume conservation if it is based on an exactly conservative VOF approach. Here, the VOF function is advected by the method of Youngs [13], which is volume conserving. For the LS function, the spatial derivatives in Equation (26) were discretized using a second-order accurate, essentially nonoscillatory scheme and the forward Euler scheme was used to discretize the temporal derivative.

The unit normal vector and curvature at any point on the interface are calculated from ϕ via

$$\hat{n}=\frac{\nabla\phi}{|\nabla\phi|} \tag{29}$$

and

$$\kappa=-\nabla\cdot\left(\frac{\nabla\phi}{|\nabla\phi|}\right) \tag{30}$$

3.3. Discretization of the Dirac delta function

As we will show in Section 4, the choice of discretization of the Dirac delta function δ_Γ has a significant impact on the accuracy of the results. The implicit surface tension model requires a

DOI: 10.1002/fld

smooth δ_Γ to minimize errors when Equation (19) or (22) is integrated over a control volume. To construct the discretized delta function, denoted by δ_ε, we used the distance function ϕ available using the CLSVOF method. If using only the VOF method, one could utilize the method described in [14] to construct ϕ from the volume fractions. We then define δ_ε as

$$\delta_\varepsilon(\phi)=\begin{cases}\dfrac{1}{\varepsilon}f(\phi/\varepsilon), & |\phi|\leqslant\varepsilon\\ 0, & |\phi|>\varepsilon\end{cases} \tag{31}$$

where f is a kernel function and $\varepsilon=m\Delta x$, where m is a positive number that determines the support of δ_ε (δ_ε becomes smoother with increasing m). We will examine the following linear, cosine and polynomial kernel functions [2] with various values of m:

$$f_{\text{linear}}(x)=1-|x| \tag{32}$$

$$f_{\cos}(x)=\tfrac{1}{2}(1+\cos(\pi x)) \tag{33}$$

$$f_{\text{poly}}(x)=\tfrac{35}{32}(1-3x^2+3x^4-x^6) \tag{34}$$

For the explicit models, we used a sharp delta function evaluated as the gradient of the volume fractions [9].

4. RESULTS

The remainder of this paper presents a comparison between the implicit surface tension model and two explicit models: the original [1] and consistent [9] CSF. The results of the consistent model are considered as benchmarks because of a more accurate representation of surface tension forces, which is due to the consistent treatment of surface tension and pressure. Unless otherwise mentioned, the results of the implicit model were obtained by using Equation (14) (backward Euler scheme) with δ_ε evaluated with the $f_{\cos}$ kernel and $m=3.5$. We adopted test cases from [2], but changed parameters such as viscosity (which is modeled explicitly here) to obtain a wide range of Δt larger than Δt_{ST} and smaller than other timestep restrictions. The parameters are all in SI units.

4.1. Static drop in the absence of gravity

First, we consider a circular static drop of radius R in zero gravity. We will present the magnitudes of dimensionless spurious currents $\mathbf{U}\mu/\sigma$, which are velocities induced due to discretization errors of the surface tension term, and the pressure jump across the interface evaluated in three ways: Δp_{total} denotes the difference between average pressures in $r\leqslant R$ and $r>R$ regions; $\Delta p_{\text{partial}}$ represents the difference between average pressures in $r\leqslant R/2$ and $r>3R/2$ regions (this avoids the transition region near the interface); $\Delta p_{\max}$ is the difference between the maximum and minimum pressures in the domain.

Consider a drop of fluid 1 with $R=0.25$ centered within a 1×1 domain otherwise filled with fluid 2. $\rho_1=\rho_2=10^3$, $\mu_1=\mu_2=5\times10^{-2}$, $\sigma=0.1$. $\Delta x=\Delta y=\frac{1}{128}$. This corresponds to an Ohnesorge number $Oh=\mu/\sqrt{2R\rho\sigma}=7\times10^{-3}$. According to the surface tension and viscous timestep restrictions (Equations (1) and (2)), $\Delta t_{\text{ST}}=0.03$ and $\Delta t_{\text{vis.}}=0.61$.

DOI: 10.1002/fld

Table I. Spurious currents, Δp at $t=90$, and time-averaged Δp, for a static drop of radius 0.25 centered within a 1×1 domain, using the original [1] and consistent explicit CSF [9] models.

	$\lvert\mathbf{U}\mu/\sigma\rvert_{\max}$	$\lvert\mathbf{U}\mu/\sigma\rvert_{\text{ave.}}$	$\Delta p_{\text{partial}}$	Δp_{total}	$\Delta p_{\max}$	$\overline{\Delta p}_{\text{partial}}$
Original CSF	1.43×10^{-3}	2.1×10^{-5}	0.4008	0.3964	0.5677	0.3975
Consistent CSF	9.8×10^{-5}	4.0×10^{-6}	0.4008	0.3964	0.4088	0.3990

$\Delta x=\Delta y=\frac{1}{128}$, $\rho_1=\rho_2=10^3$, $\mu_1=\mu_2=5\times10^{-2}$, $\sigma=0.1$, $\Delta t=0.015$, $\Delta p_{\text{exact}}=0.4$.

Table II. Spurious currents, Δp at $t=90$, and time-averaged Δp, for the static drop test.

Δt	$\lvert\mathbf{U}\mu/\sigma\rvert_{\max}$	$\lvert\mathbf{U}\mu/\sigma\rvert_{\text{ave.}}$	$\Delta p_{\text{partial}}$	Δp_{total}	$\Delta p_{\max}$	$\overline{\Delta p}_{\text{partial}}$
0.015	3.85×10^{-4}	2.30×10^{-5}	0.4073	0.3908	0.4683	0.3999
0.03	4.18×10^{-4}	2.62×10^{-5}	0.4162	0.3987	0.4469	0.3996
0.06	5.25×10^{-4}	3.65×10^{-5}	0.4025	0.3864	0.4193	0.3991
0.12	9.70×10^{-4}	5.95×10^{-5}	0.3959	0.3837	0.4014	0.3978
0.18	1.41×10^{-3}	8.20×10^{-5}	0.3962	0.3804	0.4009	0.3959

Results are for the implicit model of Equation (14) and $f_{\cos}$ with $m=3.5$, at different Δt. $\Delta t_{\text{ST}}=0.03$, $\Delta p_{\text{exact}}=0.4$.

We first used the explicit models and ran the simulations to $t=90$ with $\Delta t=0.015$. Table I shows the maximum and average magnitudes of spurious currents and the pressure jumps at $t=90$, as well as a time-averaged pressure jump denoted by a bar, where $\Delta p_{\text{exact}}=0.4$. The consistent CSF model yields much smaller spurious currents, but the pressure jumps predicted by the original and consistent CSF models are the same except for $\Delta p_{\max}$. We ran the simulations further to $t=900$, and the results (not presented) are more or less the same as the results at $t=90$.

Note that when the explicit models are used it is sometimes possible to obtain stable solutions even when the timestep is $2\Delta t_{\text{ST}}$. In fact, the way the Δt_{ST} constraint was devised [1] allows for this. We successfully ran the above test at $\Delta t=2\Delta t_{\text{ST}}$ using the consistent CSF model. However, for $\Delta t>2\Delta t_{\text{ST}}$, the explicit surface tension models failed, as expected. For example, when the original and consistent CSF models were run at $\Delta t=6\Delta t_{\text{ST}}$, the solutions became unstable after only eight and four timesteps, respectively, as velocities induced by surface tension violated the CFL condition.

Next, we ran the same simulation but with the implicit model; this time, however, we tried a range of timesteps $\Delta t=0.015$, 0.03, 0.06, 0.12, and 0.18, corresponding to $\Delta t\leqslant6\Delta t_{\text{ST}}$. Solutions were stable for all Δt. The results are presented in Table II.

Comparing the results at $\Delta t=0.015$ with those of the explicit models (Table I), the implicit model yields maximum spurious currents between those of the two explicit models (the consistent CSF model produces the smallest spurious currents). However, the average spurious currents of the implicit model are greater than those of the original CSF model. This can be explained by considering Figure 1, which shows the spurious currents induced in the flow at $t=90$, for the different surface tension models. When the original CSF model is used, the spurious currents, shown in Figure 1(c), are very large on the interface but quite small off the interface. The implicit

DOI: 10.1002/fld

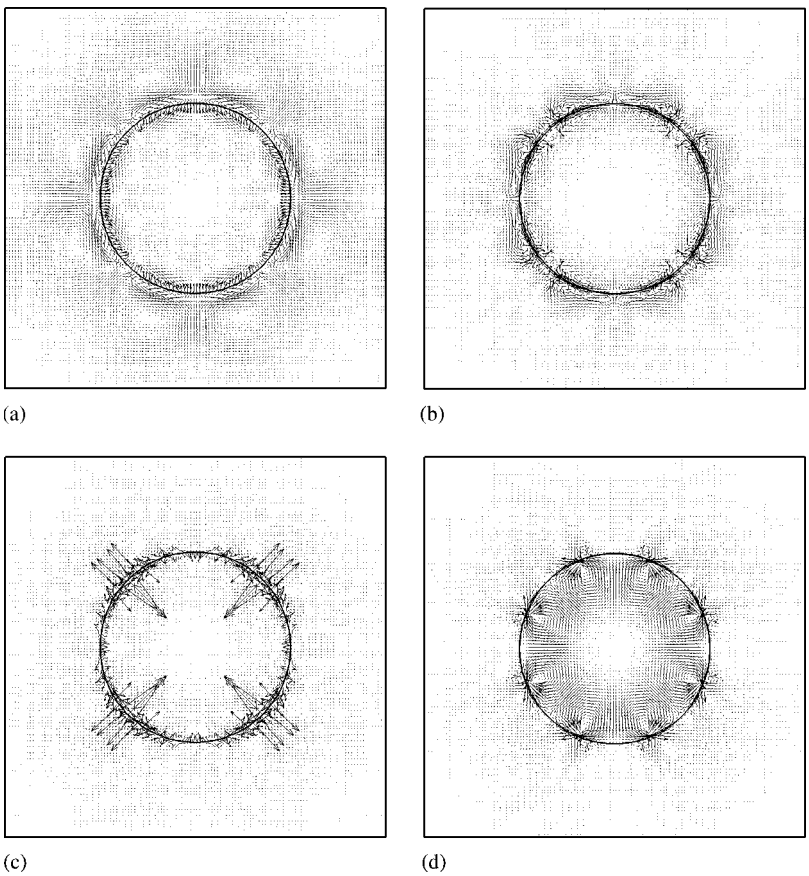

Figure 1. Spurious currents at $t=90$, for a static drop of radius 0.25 centered within a 1×1 domain. $\Delta x=\Delta y=\frac{1}{128}$, $\rho_1=\rho_2=10^3$, $\mu_1=\mu_2=5\times10^{-2}$, $\sigma=0.1$. Implicit results are of Equation (14) using $f_{\cos}$ with $m=3.5$, at (a) $\Delta t=0.18$ and (b) $\Delta t=0.015$. Explicit results are of (c) the original CSF model and (d) the consistent CSF model (velocities magnified six times), with $\Delta t=0.015$.

model (Figures 1(a) and (b)), on the other hand, yields currents that are more uniformly distributed throughout the domain. This may be because the support of the delta function is larger in the implicit model than in the explicit model. Thus, the surface tension force is distributed over a larger region around the interface, which yields greater spurious currents in that area. The diffusive operator, however, tends to align the surface tension-induced velocities along the interface. Figure 1(d) shows the consistent CSF model results magnified six times; as can be seen, spurious currents are larger on the interface and inside the drop, than outside.

Regarding runtime, using the original CSF, consistent CSF, and the implicit model, simulations ran for 175, 170, and 177 min, respectively, at $\Delta t=0.015$, suggesting that the time spent on the iterative solution of Equation (19) is insignificant. This is because these equations are solved only in cells near an interface, where surface tension effects are present. The computation time was only 19 min using the implicit model at $\Delta t=0.18$.

DOI: 10.1002/fld

Table III. Spurious currents, Δp at $t=90$, and time-averaged Δp, for the static drop test.

Δt	$\lvert\mathbf{U}\mu/\sigma\rvert_{\max}$	$\lvert\mathbf{U}\mu/\sigma\rvert_{\text{ave.}}$	$\Delta p_{\text{partial}}$	Δp_{total}	$\Delta p_{\max}$	$\overline{\Delta p}_{\text{partial}}$
0.015	3.57×10^{-4}	2.14×10^{-5}	0.3846	0.3707	0.4618	0.3999
0.03	3.41×10^{-4}	2.11×10^{-5}	0.4245	0.4062	0.4573	0.3996
0.06	5.20×10^{-4}	3.70×10^{-5}	0.3993	0.3837	0.4068	0.3992
0.12	9.10×10^{-4}	6.00×10^{-5}	0.3978	0.3800	0.4025	0.3977
0.18	1.42×10^{-3}	8.75×10^{-5}	0.3980	0.3823	0.4028	0.3981

Results are for the implicit model of Equation (16) and $f_{\cos}$ with $m=3.5$, at different Δt. $\Delta t_{\text{ST}}=0.03$, $\Delta p_{\text{exact}}=0.4$.

Table IV. Spurious currents, Δp at $t=90$, and time-averaged Δp, for the static drop test.

Δt	$\lvert\mathbf{U}\mu/\sigma\rvert_{\max}$	$\lvert\mathbf{U}\mu/\sigma\rvert_{\text{ave.}}$	$\Delta p_{\text{partial}}$	Δp_{total}	$\Delta p_{\max}$	$\overline{\Delta p}_{\text{partial}}$
0.015	1.39×10^{-3}	1.15×10^{-4}	0.3794	0.3759	0.6316	0.3959
0.03	1.36×10^{-3}	1.37×10^{-4}	0.4060	0.4013	0.5628	0.3938
0.06	1.27×10^{-3}	1.49×10^{-4}	0.3864	0.3812	0.5126	0.3801
0.12	1.30×10^{-3}	1.12×10^{-4}	0.3689	0.3625	0.4524	0.3533
0.18	1.07×10^{-3}	5.80×10^{-5}	0.3226	0.3161	0.3687	0.3230

Results are for the implicit model of Equation (14) and $f_{\cos}$ with $m=1.5$, at different Δt. $\Delta t_{\text{ST}}=0.03$, $\Delta p_{\text{exact}}=0.4$.

Next, we evaluated the implicit model of Equation (16) (the Crank–Nicolson scheme) with the same delta function. The results, presented in Table III, are very close to those of Equation (14) (see Table II); the magnitude of spurious currents and the pressure jumps are generally the same. As the results using Equation (16) are not significantly different from those using Equation (14), in this test (and others), we only present results of the Euler scheme (Equation (14)) from here on.

We next examined the effect of varying the support of the Dirac delta function. Using the implicit model and $f_{\cos}$, we tried $m=1.5$ (a 3-cell wide delta function) and ran the same test. The results are presented in Table IV; as can be seen, the spurious currents are larger compared with the smoother delta function ($m=3.5$, see Table II). Furthermore, the pressure jumps decrease as Δt increases. We observed [15] the same behavior with a sharp delta function constructed from the volume fractions, where the loss in pressure jump was less severe when the Crank–Nicolson scheme was used.

The loss in pressure jump occurs because of errors that result from integrating the sharp delta function (Equation (19) or (22)) over control volumes. In our finite volume implementation, similar to other quantities such as pressure, the delta function is assumed to be constant across a cell (control volume), and is represented by the value at the cell center. For a sharply varying function, this assumption induces large errors that can be reduced by using a smoother delta function.

Finally, we studied the performance of the other kernels (linear equation (32) and polynomial equation (34)), with $m=3.5$. Table V shows the results; compared with the cosine kernel (Table II),

DOI: 10.1002/fld

Table V. Spurious currents, Δp at $t=90$, and time-averaged Δp, for the static drop test.

Δt	$\lvert\mathbf{U}\mu/\sigma\rvert_{\max}$	$\lvert\mathbf{U}\mu/\sigma\rvert_{\text{ave.}}$	$\Delta p_{\text{partial}}$	Δp_{total}	$\Delta p_{\max}$	$\overline{\Delta p}_{\text{partial}}$
(a)						
0.015	4.88×10^{-4}	2.59×10^{-5}	0.3700	0.3554	0.4436	0.3991
0.03	4.56×10^{-4}	2.86×10^{-5}	0.3990	0.3816	0.4424	0.3987
0.06	3.24×10^{-4}	2.39×10^{-5}	0.3984	0.3808	0.4086	0.3983
0.12	2.43×10^{-4}	2.48×10^{-5}	0.3974	0.3796	0.4033	0.3973
0.18	2.01×10^{-4}	2.56×10^{-5}	0.3960	0.3781	0.4010	0.3959
(b)						
0.015	4.05×10^{-4}	2.30×10^{-5}	0.3991	0.3850	0.4498	0.4001
0.03	4.54×10^{-4}	2.66×10^{-5}	0.4047	0.3899	0.4383	0.3998
0.06	5.70×10^{-4}	3.88×10^{-5}	0.4086	0.3936	0.4354	0.3990
0.12	1.08×10^{-3}	6.35×10^{-5}	0.3981	0.3837	0.4044	0.3972
0.18	2.94×10^{-4}	3.70×10^{-5}	0.3944	0.3800	0.3999	0.3947

Results are for the implicit surface tension model of Equation (14) using (a) f_{linear} and (b) f_{poly}, with $m=3.5$, at different Δt. $\Delta t_{\text{ST}}=0.03$, $\Delta p_{\text{exact}}=0.4$.

the different kernels generally yield similar results; using the linear kernel, however, the magnitude of spurious currents is slightly smaller, when $\Delta t>\Delta t_{\text{ST}}$.

4.2. Surface tension-driven oscillation

Next, we present the results of the oscillation of a drop due to surface tension effects. The initial geometry is an ellipse with semimajor axes of 0.3 and 0.2 in the x- and y-directions, respectively. We ran the simulation to $t=1000$; the same timestep restrictions as presented in Section 4.1 apply here, as the fluid properties and mesh resolution are the same. We studied four cases: the implicit and two explicit (original and consistent CSF) models at $\Delta t=0.015$, and the implicit model at $\Delta t=0.18=6\Delta t_{\text{ST}}$.

The results of the implicit model with $\Delta t=0.18$ are presented in Figure 2. The results are stable and the oscillations cease at $t=300$. Figure 3 depicts the history of the total kinetic energy of the flow, measured over the whole domain, for $0\leqslant t\leqslant 300$, for the different models. The amplitude and frequency of the oscillations are quite similar when the explicit models are used; the implicit model with $\Delta t=0.18$ yields similar results in terms of the amplitude of oscillations, but the frequency differs very slightly for $t>100$. For $\Delta t=0.015$, the frequency of the implicit results matches the frequency of the explicit results; however, we observe a slightly larger amplitude in the results of the implicit model. The small differences between the results of the implicit and explicit models may be due to the different representation of the surface tension force, which results in a different balance between surface tension and pressure forces. As can be seen in Figure 3, the amplitudes of the consistent CSF model are also slightly greater than those of the original CSF model for $t>100$; this is due to a more accurate representation of surface tension forces in the consistent model.

Figure 4 shows the history of the viscous dissipation $\Phi=(\mu/2)(\partial u_i/\partial x_j+\partial u_j/\partial x_i)^2$ in the flow, for the implicit result at $\Delta t=0.18$, for $0\leqslant t\leqslant 300$. The frequency of oscillation in Figure 4 is similar to that of the total kinetic energy in Figure 3.

DOI: 10.1002/fld

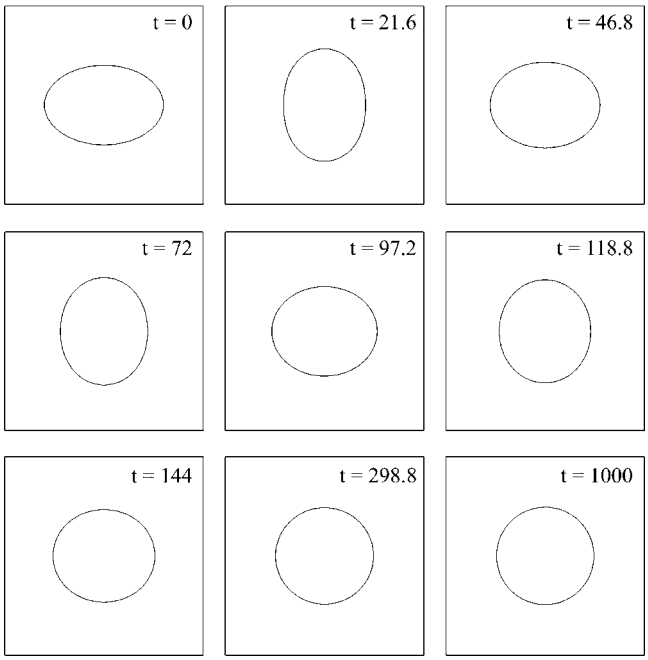

Figure 2. Interface shape as a drop oscillates due to surface tension effects. $\Delta t = 0.18$, $\Delta x = \Delta y = \frac{1}{128}$, $\rho_1 = \rho_2 = 10^3$, $\mu_1 = \mu_2 = 5 \times 10^{-2}$, $\sigma = 0.1$, $\Delta t_{\mathrm{ST}} = 0.03$. The implicit surface tension model of Equation (14) is used with $f_{\cos}$ and $m = 3.5$.

4.3. Buoyancy-driven flow

Finally, we consider a bubble of fluid 1 with radius $R = 0.1$ positioned at (0.5,0.5) in a 1×2 container otherwise filled with fluid 2. $\rho_1 = 500$, $\rho_2 = 10^3$, $\mu_1 = \mu_2 = 10^{-2}$, $\sigma = 0.1$, $g = -9.81 \times 10^{-3}$, and $\Delta x = \Delta y = \frac{1}{128}$. This corresponds to $Oh_1 = 3 \times 10^{-3}$ and a Bond number $Bo_1 = 4\rho_1 g R^2/\sigma = 1.96$. The surface tension and viscous timestep restrictions are $\Delta t_{\mathrm{ST}} = 0.024$ and $\Delta t_{\mathrm{vis.}} = 1.53$. Note that gravity was assigned a small value here to obtain a wide range of Δt, larger than Δt_{ST}, but small enough to ensure CFL numbers less than unity even for the largest buoyancy-induced velocities.

We simulated the buoyancy-driven motion of the bubble using the implicit and explicit models. Figure 5(a) illustrates bubble shapes at $t = 0$, 15, and 30 obtained by the implicit model with $\Delta t = 0.12 = 5\Delta t_{\mathrm{ST}}$; Figure 5 also shows results with $\Delta t = 0.012$ using the implicit and explicit models. The results are quite similar in terms of bubble height and shape. To compare, all of the bubble shapes at $t = 30$ are superimposed in Figure 6. Note that the interface shapes predicted by the explicit models differ; this is due to the more accurate treatment of surface tension in the consistent CSF model. Results of the implicit model at $\Delta t = 0.012$ are close to those of the original CSF model. Using $\Delta t = 0.12$, however, the height of the bubble is slightly above that obtained using a smaller timestep, and the bubble is less deformed. The differences are due to the transient nature of the problem; with $\Delta t = 0.12$, the implicit model captures temporal attributes less accurately because Δt is large. As we decrease Δt, results of the implicit model become closer

DOI: 10.1002/fld

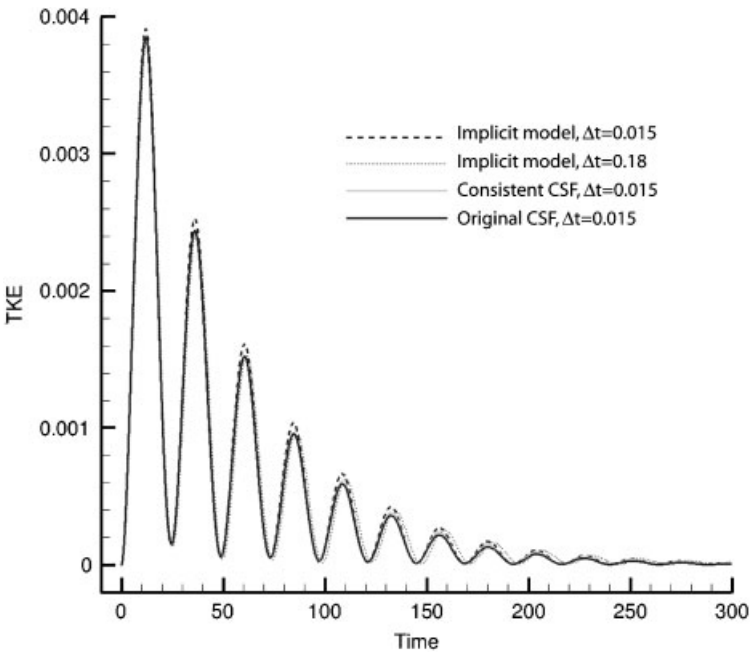

Figure 3. The history of the total kinetic energy (TKE) in an oscillating drop. Results are of the original and consistent CSF models, and of the implicit model, all at $\Delta t = 0.015$, and of the implicit model at $\Delta t = 0.18$; $\Delta t_{ST} = 0.03$.

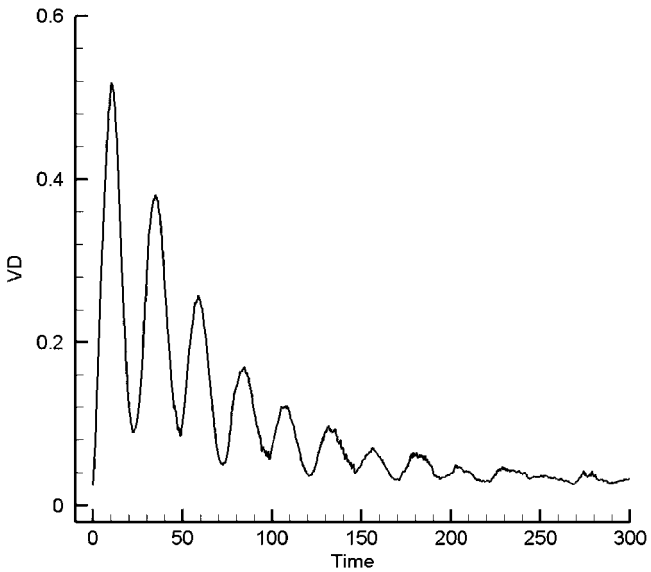

Figure 4. The history of the viscous dissipation (VD) in an oscillating drop. Results are of the implicit model with $\Delta t = 0.18$; $\Delta t_{ST} = 0.03$.

DOI: 10.1002/fld

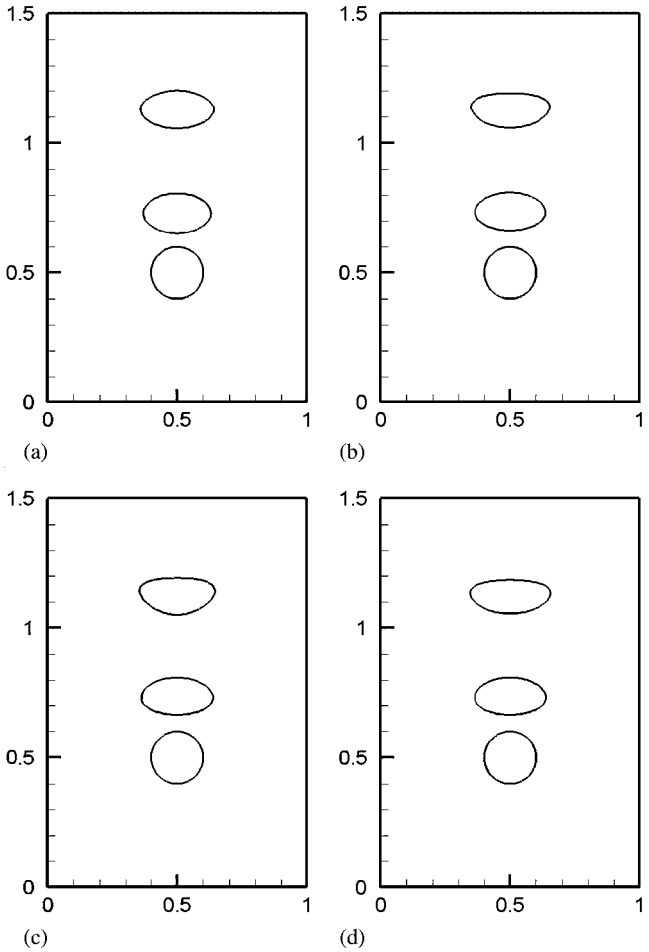

Figure 5. Interface shape as a bubble (fluid 1) rises in fluid 2 due to buoyancy forces, at $t=0$, 15, and 30. $\rho_1=500$, $\rho_2=1000$, $\mu_1=\mu_2=10^{-2}$, $\sigma=0.1$, $g=-9.81\times10^{-3}$, $\Delta x=\Delta y=\frac{1}{128}$, $\Delta t_{\mathrm{ST}}=0.024$. Implicit results are based on Equation (14), with $f_{\cos}$ and $m=3.5$, at (a) $\Delta t=0.12$, and (b) $\Delta t=0.012$. Explicit results are of the (c) original and (d) consistent CSF models with $\Delta t=0.012$.

to those of the explicit models. The differences become insignificant as we refine the mesh, where a much smaller Δt is required.

5. SUMMARY

The surface tension timestep restriction associated with the explicit CSF model is stringent, especially when surface tension is a dominant force. Hysing [2] reported a semi-implicit CSF model in a finite element context that mitigates the timestep restriction significantly. Here, we presented an implementation of Hysing's model for interfacial flows modeled by a finite volume method.

DOI: 10.1002/fld

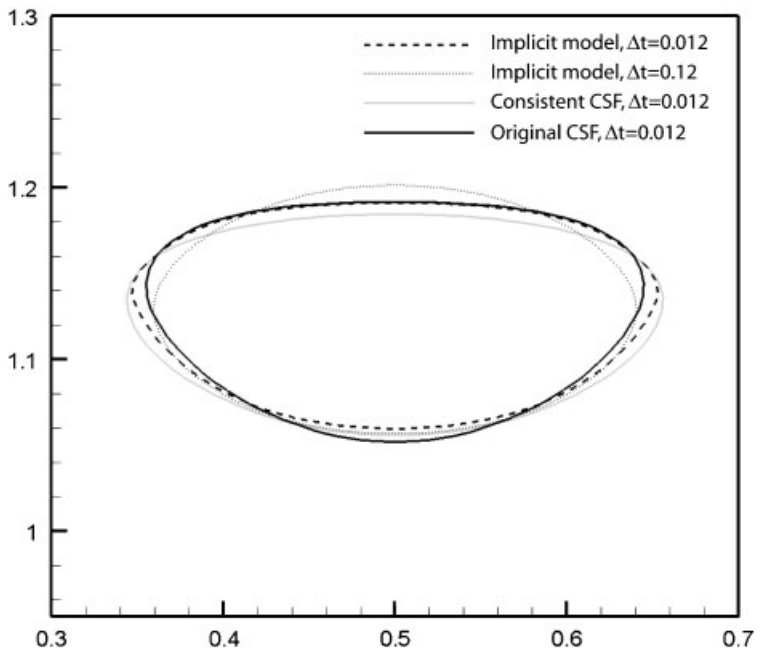

Figure 6. Bubble shape at $t=30$ obtained from the original and consistent CSF models with $\Delta t=0.012$, and from the implicit model of Equation (14), with $f_{\cos}$ and $m=3.5$, with $\Delta t=0.012$ and $\Delta t=0.12$; $\Delta t_{\mathrm{ST}}=0.024$.

In this implementation, the surface tension force consists of an explicit part, which is the regular CSF, and an implicit part which represents the diffusion of velocities induced by surface tension on fluids interfaces. The solution of velocities induced by surface tension involves an iterative procedure for cells near an interface; the computational time spent on the iterative procedure is insignificant. Results show that using the implicit model, the timestep restriction due to surface tension can be exceeded by at least a factor of 5, without destabilizing the numerical solution. This would significantly reduce simulation runtimes by time marching at larger timesteps. The results of the implicit model at large timesteps are very similar to those of the explicit models. Similar to [2], because of the explicit part of the surface tension force, the maximum Δt possible is limited.

APPENDIX A

A.1. Tangential gradient

The tangential gradient of a scalar function f is defined as

$$\underline{\nabla} f=\nabla f-(\hat{n}\cdot\nabla f)\hat{n} \tag{A1}$$

where ∇ denotes the regular gradient, and $\hat{n}$ is the unit normal vector to the surface on which the tangential gradient is calculated. The tangential gradient is then the directional derivative of f in the direction tangent to a surface.

DOI: 10.1002/fld

In 2D Cartesian coordinates, where $f = f(x, y)$ and $\hat{n} = n_1\hat{i} + n_2\hat{j}$, the tangential gradient is

$$\underline{\nabla} f = (f_x\hat{i} + f_y\hat{j}) - (n_1 f_x + n_2 f_y)(n_1\hat{i} + n_2\hat{j}) \tag{A2}$$

or

$$\underline{\nabla} f = (f_x - n_1(n_1 f_x + n_2 f_y))\hat{i} + (f_y - n_2(n_1 f_x + n_2 f_y))\hat{j} \tag{A3}$$

where the subscripts x and y denote differentiation with respect to x and y, respectively.

A.2. Tangential Laplacian

The tangential Laplacian or Laplace–Beltrami operator of f is defined as

$$\begin{aligned}\underline{\Delta} f &= \underline{\nabla} \cdot \underline{\nabla} f \\ &= \nabla \cdot \underline{\nabla} f - (\hat{n} \cdot \nabla)(\underline{\nabla} f) \cdot \hat{n}\end{aligned} \tag{A4}$$

In 2D, the first term in Equation (A4) is

$$\nabla \cdot \underline{\nabla} f = \nabla \cdot ((f_x - n_1(\underbrace{n_1 f_x + n_2 f_y}_{=A}))\hat{i} + (f_y - n_2(n_1 f_x + n_2 f_y))\hat{j})$$

$$= f_{xx} - n_{1x}A - n_1 A_x + f_{yy} - n_{2y}A - n_2 A_y \tag{A5}$$

In the second term of Equation (A4)

$$\begin{aligned}(\hat{n} \cdot \nabla)(\underline{\nabla} f) &= n_1 \frac{\partial}{\partial x}(f_x - n_1 A)\hat{i} + n_2 \frac{\partial}{\partial y}(f_x - n_1 A)\hat{i} \\ &\quad + n_1 \frac{\partial}{\partial x}(f_y - n_2 A)\hat{j} + n_2 \frac{\partial}{\partial y}(f_y - n_2 A)\hat{j} \\ &= (n_1 f_{xx} - n_1(n_{1x}A + n_1 A_x) + n_2 f_{xy} - n_2(n_{1y}A + n_1 A_y))\hat{i} \\ &\quad + (n_1 f_{xy} - n_1(n_{2x}A + n_2 A_x) + n_2 f_{yy} - n_2(n_{2y}A + n_2 A_y))\hat{j}\end{aligned} \tag{A6}$$

and hence,

$$\begin{aligned}(\hat{n} \cdot \nabla)(\underline{\nabla} f) \cdot \hat{n} &= n_1^2 f_{xx} - n_1^2(n_{1x}A + n_1 A_x) + n_1 n_2 f_{xy} \\ &\quad - n_1 n_2(n_{1y}A + n_1 A_y) + n_1 n_2 f_{xy} \\ &\quad - n_1 n_2(n_{2x}A + n_2 A_x) + n_2^2 f_{yy} - n_2^2(n_{2y}A + n_2 A_y)\end{aligned} \tag{A7}$$

Combining Equations (A5) and (A7)

$$\begin{aligned}\underline{\Delta} f &= f_{xx}(1 - n_1^2) + f_{yy}(1 - n_2^2) - 2n_1 n_2 f_{xy} - n_{1x}A(1 - n_1^2) \\ &\quad - n_1 A_x(1 - n_1^2 - n_2^2) - n_{2y}A(1 - n_2^2) - n_2 A_y(1 - n_1^2 - n_2^2) \\ &\quad + n_1 n_2 A(n_{2x} + n_{1y})\end{aligned} \tag{A8}$$

DOI: 10.1002/fld

or

$$\underline{\Delta} f = n_2^2 f_{xx} + n_1^2 f_{yy} - 2n_1 n_2 f_{xy} - (n_1 f_x + n_2 f_y)(n_1^2 n_{2y} + n_2^2 n_{1x} - n_1 n_2 (n_{2x} + n_{1y})) \tag{A9}$$

A.3. Tangential gradient and tangential Laplacian of a vector

Consider a 2D vector quantity $\mathbf{U} = u\hat{i} + v\hat{j}$. On a surface with unit normal vector $\hat{n} = n_1\hat{i} + n_2\hat{j}$, the tangential gradient and tangential Laplacian of $\mathbf{U}$ are

$$\underline{\nabla}\mathbf{U} = \begin{bmatrix} u_x & u_y \\ v_x & v_y \end{bmatrix} - \begin{bmatrix} n_1(n_1 u_x + n_2 u_y) & n_2(n_1 u_x + n_2 u_y) \\ n_1(n_1 v_x + n_2 v_y) & n_2(n_1 v_x + n_2 v_y) \end{bmatrix} \tag{A10}$$

and

$$\underline{\Delta}\mathbf{U} = \begin{bmatrix} n_2^2 u_{xx} + n_1^2 u_{yy} - 2n_1 n_2 u_{xy} \\ \quad - (n_1 u_x + n_2 u_y)(n_2^2 n_{1x} + n_1^2 n_{2y} - n_1 n_2 (n_{1y} + n_{2x})) \\ n_2^2 v_{xx} + n_1^2 v_{yy} - 2n_1 n_2 v_{xy} \\ \quad - (n_1 v_x + n_2 v_y)(n_2^2 n_{1x} + n_1^2 n_{2y} - n_1 n_2 (n_{1y} + n_{2x})) \end{bmatrix} \tag{A11}$$

ACKNOWLEDGEMENTS

The authors would like to thank Shu-Ren Hysing for helpful discussions.

REFERENCES

1. Brackbill JU, Kothe DB, Zemach C. A continuum method for modeling surface tension. *Journal of Computational Physics* 1992; **100**:335–354.
2. Hysing S. A new implicit surface tension implementation for interfacial flows. *International Journal for Numerical Methods in Fluids* 2006; **51**:659–672.
3. Turek S, Beckerand C. *FEATFLOW—Finite Element Software for the Incompressible Navier–Stokes Equations*, *User Manual*. Universität Dortmund, 1999.
4. Kothe DB, Mjolsness RC, Torrey MD. RIPPLE: a computer program for incompressible flows with free surfaces. *Technical Report LA-12007-MS*, LANL, 1991.
5. Lafaurie B, Nardone C, Scardovelli R, Zaleski S, Zanetti G. Modelling merging and fragmentation in multiphase flows with SURFER. *Journal of Computational Physics* 1994; **113**(1):134–147.
6. Popinet S. *The Gerris Flow Solver*, 2003. Available from: http://gfs.sourceforge.net/.
7. Bänsch E. Finite element discretization of the Navier–Stokes equations with a free capillary surface. *Numerische Mathematik* 2001; **88**(2):203–235.
8. Bussmann M, Kothe DB, Sicilian JM. Modeling high density ratio incompressible interfacial flows. *Proceedings of ASME 2002 Fluids Engineering Division Summer Meeting*, Montreal, Canada, 2002.
9. Francois MM, Cummins SJ, Dendy ED, Kothe DB, Sicilian JM, Williams MW. A balanced-force algorithm for continuous and sharp interfacial surface tension models within a volume tracking framework. *Journal of Computational Physics* 2006; **213**(1):141–173.
10. Skalicky T. *LASPack Reference Manual*, 1995. Available from: www.mgnet.org/mgnet/Codes/laspack/html/laspack.html.
11. Son G, Hur N. A coupled level set and volume-of-fluid method for the buoyancy-driven motion of fluid particles. *Numerical Heat Transfer*, *Part B* 2002; **42**:523–542.

DOI: 10.1002/fld

12. Osher S, Fedkiw R. *Level Set Methods and Dynamic Implicit Surfaces*. Springer: New York, 2003.
13. Youngs DL. Time-dependent multi-material flow with large fluid distortion. In *Numerical Methods for Fluid Dynamics*, Morton KW, Baines MJ (eds). Academic Press: New York, 1982; 273–285.
14. Cummins SJ, Francois MM, Kothe DB. Estimating curvature from volume fractions. *Computers and Structures* 2005; **83**:425–434.
15. Raessi M, Bussmann M, Mostaghimi J. An implicit implementation of surface tension in finite volume models for two-phase flows. *Twentieth Annual Conference on Liquid Atomization and Spray Systems*, Chicago, IL, 2007.

DOI: 10.1002/fld